Available online at www.sciencedirect.com
SCIENCE DIRECT®
Journal of Power Sources 118 (2003) 237–247
JOURNAL OF POWER SOURCES
www.elsevier.com/locate/jpowsour

Electrolytic hydrogen storage in reluctant intermetallic systems

U. Casellato[a], N. Comisso[b], G. Davolio[c], G. Mengoli[b,*]

[a]CNR ICIS, Corso Stati Uniti 4, 35127 Padova, Italy
[b]CNR IENI, Corso Stati Uniti 4, 35127 Padova, Italy
[c]Università di Modena, Dip. di Chimica, Via Campi 183, 41100 Modena, Italy

Abstract

Composite electrodes were prepared by mixing, in the ratio 60/40 by weight, the powder of an electrochemically inhibited intermetallic compound (IMC), e.g. TiFe 50/50, TiNi 70/30 or TiNi 40/60 (alloy precursor grade) with Fe powder and pressing the mixture on to a Ni foam support. The charge capacity achieved in these composites was then compared with the capacity of ''blank'' electrodes in which the IMC had been replaced by an inactive metal (Ti or Ni). The blanks attained capacities in the range 150–200 mA h g^{-1}, although these values were largely exceeded by some IMC + Fe composites due, presumably, to storage on hydrogen. The electrocatalytic properties of Fe are probably not sufficient to explain the activation of hydrogen absorption in the inhibited IMC, since X-ray and energy-dispersive analysis (EDAX) of activated samples did reveal that deep modifications occurred in some composites, in which the formation of new phases may have been induced by charging–discharging cycles.

Keywords: Intermetallic compounds; Hydrogen storage; Electrolytic hydriding

1. Introduction

Intermetallic compounds (IMCs) which, over wide ranges of composition and/or stoichiometry, can absorb large amounts of gaseous hydrogen, are practically infinite in number: even those which have nearly flat hydrogen absorption–desorption isotherms, with both slightly negative hydriding enthalpies and decomposition pressures not far from atmospheric, are still very numerous.

In theory, the latter can not only absorb hydrogen electrolytically, but also potentially represent the negative electrodes of batteries for charge (hydrogen) storage [1,2]. However, thermodynamic features favourable to electrolytic hydriding, as determined by gas loading in (quasi) equilibrium conditions, do not necessarily match the dynamic conditions of electrolytic charging–discharging cycles [1]; again, in aqueous alkaline electrolytes, IMCs usually face serious passivity or corrosion phenomena which do not occur in solid–gas systems.

In alkaline media, the constitution of surface oxides resistant to electrochemical reduction or the progressive corrosion of less noble components do cause many IMCs either to be totally reluctant towards electrolytic hydriding or to have a very limited cycling life.

Nevertheless, several successful routes have recently been found to render some IMCs suitable for electrolytic hydriding and eventually capable of high electrochemical performance as negative electrodes in widely marketed batteries [3–5].

The most frequently followed route involves modifying the original alloy composition (A_nB_m) [1–4] by partial replacement of A, B, or both, with a third, fourth or fifth element: the substitutional atom may affect either the bulk properties of the IMCs, like lattice constants, or interfacial behaviour, such as corrosion resistance, rate and mechanism of the hydrogen evolution reaction (her), etc. [1–4]. For instance, $LaNi_5$ (AB_5) considered a superior candidate for Ni-metal hydride batteries, in practice shows an exponential decline in charge (hydrogen) capacity with number of cycles, whereas the progressive modification of the original composition into $La_{0.8}Nd_{0.2}Ni_{2.5}Co_{2.2}Si_{0.8}$ leads to more than 5×10^3 charging–discharging cycles without significant capacity loss [1]. Partial substitution in the alloy formula has also been successfully adopted for Ti_nNi_m (AB and A_2B) IMCs by replacing some Ti with Zr and V [6] or some Ni with Co [7].

Other routes to make IMCs feasible for electrolytic hydrogen storage comprise: encapsulation of the original compound by an electrodeposited foreign metal layer [2,3,8]; mechanical grinding of the IMC with an unbound element (the hydrogen capacity of a passive Mg_2Ni type

* Corresponding author. Fax: +39-049-8295853.
E-mail address: giuliano.mengoli@ieni.cnr.it (G. Mengoli).

0378-7753/03/$ – see front matter © 2003 Elsevier Science B.V. All rights reserved.
doi:10.1016/S0378-7753(03)00089-2

alloy is increased by grinding with Ni to >500 mA h g^{-1} [9]); binding of AB_2 and AB_5 compounds with Teflonized carbon additives [10].

The present work deals with an alternative activation procedure, which basically consists of loading the IMC powder used for electrode fabrication with large amounts of active Fe powder, which is expected to improve the interfacial behaviour of the material.

Fe was chosen for its potential proximity to both reactions [11]: as well as for its large capacity in reaction II) whereby, if there is physical–chemical compatibility

$$IMCH_x + xOH^- \rightleftharpoons IMC + xH_2O + xe^- \quad (I)$$

$$Fe + 2OH^- \rightleftharpoons Fe(OH)_2 + 2e^- \quad (II)$$

between Fe and the chosen IMC, a synergetic contribution to the specific capacity of the overall material may be expected.

2. Experimental

2.1. Materials

Fe powder of sizes ≤100 μm was SNDC-NIFE material, especially designed for commercial Ni–Fe batteries; Ni of ≤200 μm and Ti powders of ≤150 μm were 99.5% purity metals from Goodfellow. IMC powders were from two sources: Ti_2Ni (in stoichiometric ratio) of ≤300 μm true IMC, and $Ti_{40}Ni_{60}$ (in weight proportion) of ≤150 μm, alloy precursor grade, were from Goodfellow; TiFe (in stoichiometric ratio) of ≤50 μm and $Ti_{70}Ni_{30}$ (in weight proportion) of ≤50 μm were both alloy grade from Alfa (Johnson–Mattey).

Chemicals used for electrolytic solutions were KOH and LiOH reagent grade from Fluka and H_2O of Millipore grade: the typical electrolyte consisted of KOH 4 M + LiOH 2 M, as recommended for Ni–Fe batteries [12,13]. N_2 was 99.9% purity gas from SIO.

2.2. Apparatus and procedure

The metal powders were made suitable for electrochemical investigation by inserting a weighed amount of powder on to a weighed strip of Ni foam (which acted as powder support), followed by pressing at 100–300 atm, fixing by immersion in a diluted solution of epoxy resin and drying in hot air; the powder content (active material) of each strip was between 70 and 80% of the total weight. Sample electrodes were fabricated by cutting squares from a larger strip, which were then pressure-bonded to a Ni wire composing the electrical connection from the electrolyte to the outside.

Table 1 gives the characteristics (composition, weight, dimensions) of these electrodes. The first sample (A) contained Fe only; the active materials in the others (B–L) were two-component mixtures of powders, 60% (by weight) of the selected metal or IMC and 40% of Fe. These fixed proportions allowed comparative evaluation of the charge storage on hydrogen, if any, contributed by each IMC.

Table 1
Characteristics of the prepared electrodes

Electrode	Composition (% by weight)	Dimensions (cm^3)	Net weight (g)	Fe content (g)
A	Fe 100	2.00 × 0.75 × 0.04	0.199	0.199
B	Ni 60 + Fe 40	2.00 × 0.80 × 0.04	0.202	0.081
C	Ti 60 + Fe 40	2.00 × 0.65 × 0.04	0.174	0.070
D	Ti_2Ni 60 + Fe 40	2.00 × 0.70 × 0.04	0.207	0.083
E	TiFe 60 + Fe 40	2.00 × 0.70 × 0.04	0.200	0.080
F	TiFe 60 + Fe 40	2.00 × 0.70 × 0.04	0.174	0.070
G	($Ti_{40}Ni_{60}$) 60 + Fe 40	2.00 × 0.80 × 0.04	0.220	0.088
H	($Ti_{40}Ni_{60}$) 60 + Fe 40	2.00 × 0.65 × 0.04	0.201	0.080
I	($Ti_{70}Ni_{30}$) 60 + Fe 40	2.00 × 0.70 × 0.04	0.191	0.076
L	($Ti_{70}Ni_{30}$) 60 + Fe 40	2.00 × 0.80 × 0.04	0.196	0.078

The pressed powder sample constituted the working electrode; the counter electrode was a Ni coil (diameter = 0.1 cm, length = 100 cm) rolled around the former; the reference electrode was Hg|HgO 0.1 M KOH (manufactured by AMEL). This three electrode system was supported by the Teflon lid of a cylindrical uncompartmented polyethylene cell of 150 cm^3 capacity. The cell was equipped with an inlet–outlet pipe system which allowed the gas produced during electrolysis to be removed by a N_2 flow. All experiments were carried out at room temperature (23 ± 2 °C).

Electrochemical instrumentation consisted of AMEL apparatus interfaced with a PC which automatically recorded the charging–discharging curves of the working electrode and integrated the current.

Some samples were analyzed both before and after the electrolytic runs by X-ray diffraction with a Philips PV 3710 instrument (Cu Kα radiation, 40 kV, 30 mA). The equipment included a silicon spinning holder and a graphite monochromator. The detection range was between 5 and 90° (2θ).

Scanning electron microscopy (SEM) observations were made on Philips XL-40 LaB_6 apparatus. Quantitative standardless microanalyses were obtained using an energy-dispersive analysis (EDAX) PV-99 X-ray spectrometer with a Be window.

3. Results

3.1. Charge storage in pure Fe (samples A–C)

The sample containing Fe only (Table 1, A) was examined first, to assess the electrochemical performance intrinsic to both the material (Fe NIFE) and its manufacture as a pressed powder electrode.

Fig. 1 shows how this electrode was progressively activated to store charge by a succession of charging–discharging cycles. The graph was built by plotting, at any cycle, the charge extracted from the first oxidation plateau of Fe (see below), by a galvanostatic current *I* of either 21 or 42 mA (to

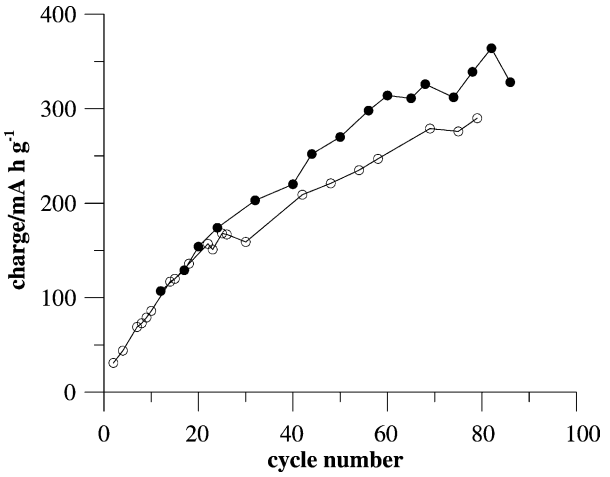

Fig. 1. Evolution of charge capacity of sample A (pure Fe powder) with the number of charging–discharging cycles. Full point: charge extracted after prolonged low current charging. Empty point: charge resulting after fast charging.

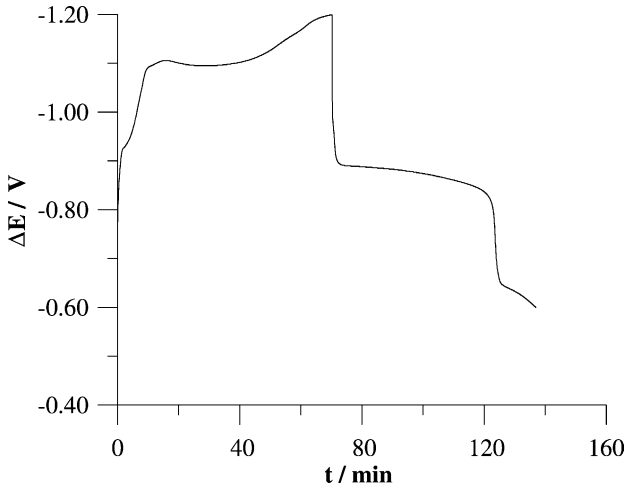

Fig. 2. ΔE vs. time pattern of sample A during a charging ($I = 42$ mA) and discharging ($I = -42$ mA) cycle.

convert I to j, milliampere per square centimetre or milliampere per gram, the electrode characteristics shown in Table 1 may be used). The empty circles represent the charge obtained after fast charging runs ($I = -200(-250)$ mA $\times$ 1 h) and the full ones the charge extracted after low current ($I = -42$ mA) charging, prolonged overnight (13–14 h). Discharging followed charging without any delay.

The activation process was quite slow: after nearly 100 cycles, the limit had not yet been achieved, but maximum storage (364 mA h g^{-1}; see Table 2), although obtained only after prolonged reduction, was comparable with that of a good sintered Fe plate. In effect, maximum storage at 25 °C of Fe plates suitable for practical application in Ni–Fe batteries was ≈1/3 of the theoretical Fe capacity (960 mA h g^{-1}) [14]. The storage considered here concerns only the charge extracted at the first oxidation stage of Fe (reaction II), which takes place along a plateau flexing at ≈−0.800 V versus HgO, but discharging was usually prolonged to the further Fe oxidation stages (−0.600/−0.500 V versus HgO). Otherwise, electrode activation was even more sluggish: this peculiarity was taken into account when activating the other sample electrodes.

Table 2
Maximum charge capacity of electrodes A–C

Electrode	Charging mode (fast/slow)	Extracted charge (mA h g^{-1})	Charge based on Fe content (mA h g^{-1})
A (pure Fe)	Fast	290	290
A (pure Fe)	Slow	364	364
B (Ni + Fe)	Fast	177	440
B (Ni + Fe)	Slow	203	508
C (Ti + Fe)	Fast	152	376
C (Ti + Fe)	Slow	171	425

Fig. 2 shows the profile of the Fe electrode potential as a function of time throughout a charging–discharging cycle carried out by galvanostatic currents of −42/42 mA. The graph was drawn by plotting the Fe single-electrode potential as potential difference ΔE (towards the reference electrode), which simulates battery behaviour better.

Other than the main Fe ⇌ Fe^{II} reaction, the more positive oxido/reduction processes of Fe are evident in both charging and discharging. For the condition shown in Fig. 2, whereby only 60% of maximum storage was driven, the coulombic efficiency of the Fe ⇌ Fe^{II} reaction was ≈75%, whereas that of the whole cycle was over 90%.

Fig. 3 shows the evolution of charge storage in samples B (Ni + Fe) and C (Ti + Fe) with the number of charging–discharging cycles. This figure was obtained in the same way as Fig. 1: the triangles refer to B, the squares to C; the

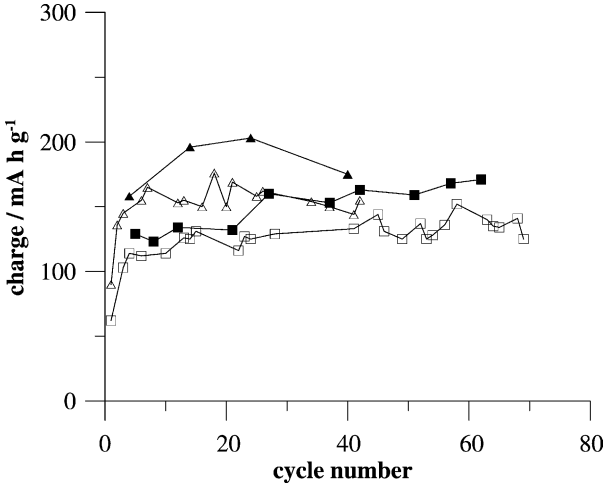

Fig. 3. Evolution of charge capacity with the number of cycles of sample B (triangles, Ni + Fe) and C (squares, Ti + Fe). Full and empty have the same meaning as in Fig. 1.

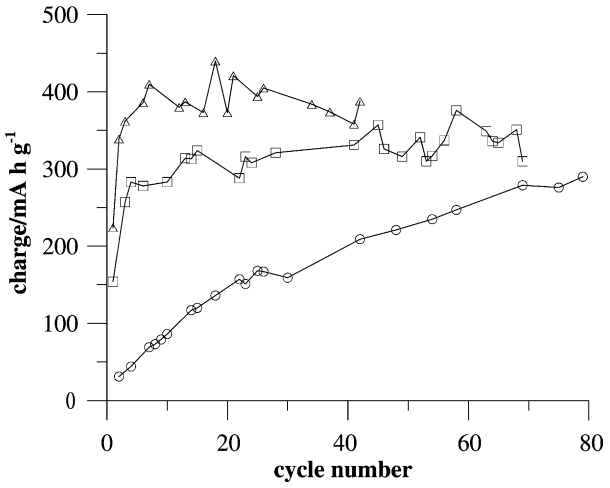

Fig. 4. Comparison of the activation patterns of sample A (circles), B (triangles) and C (squares). The capacity of samples B and C is normalised to the mere Fe content.

empty symbols again represent charges extracted after fast charging and full ones charges obtained after prolonged low current charging.

The activation of B and C thus appears to be much faster than that of A, as the limit capacity is already approached after 10–20 cycles. When these capacities are related, as in Fig. 3, to the whole powder content of the electrode, they are clearly below the values attained by sample A. However, when the same capacities are related only to the Fe of each sample, they are definitely above that of the pure Fe electrode, as shown in Table 2. Does this mean that Ni and Ti contribute towards charge storage? Fig. 4, which shows the evolution with the number of cycles of the charge capacity normalized only to the Fe content of samples A–C, may provide the answer: Fe dispersion into Ni or Ti does affect activation kinetics, but the maximum capacity of each sample probably has the same limit which—in the case of the Fe powder electrode (A) alone—is only asymptotically approached.

It is in fact unlikely that Ni and Ti were significantly engaged in hydriding which, even in the presence of Fe, is hindered either by the intrinsic instability of hydride (for Ni) or by exceedingly slow hydrogen diffusion (for Ti).

The faster activation and larger charge storage of B and C with respect to A are thus explained by the dispersion of Fe particles, so that the detrimental effect of the volumetric increase in Fe (paralleling reaction II), which shields other Fe particles from the electrochemical reaction [15], is diminished.

The ‘‘dispersion’’ effect is more efficient when extended Ni than by Ti (see Figs. 3–4). This fact may be ascribed to the catalytic activity of Ni, whereby the reduction of the most resistant Fe oxides may be partially induced by atomic hydrogen supplied by Ni particles adjacent to those of Fe. In this view, the slight decline in charge capacity with number of cycles, shown by sample B, may be explained by progressive poisoning of catalysis by Ni.

The above effects—dispersion and electrocatalytic reduction of resistive Fe oxides—must be considered when dealing with charge storage in the IMC + Fe sample electrodes.

3.2. Charge storage in mixed IMC + Fe powder electrodes

3.2.1. Behaviour of sample D (Ti_2Ni + Fe)

Before investigating charge storage in the composite, the behaviour of a pressed powder electrode containing only Ti_2Ni was examined. Non-negligible charge (≈100mA h g^{-1}) could be stored initially, but charge capacity dropped after a few cycles. This finding agrees with previous literature reports in which Ti_2Ni, used alone as hydrogen storage electrode material, deactivates quickly, owing to the formation of an irreversible $Ti_2NiH_{0.5}$ phase [16,17].

As regards the mixed Ti_2Ni + Fe electrode, the simultaneous contribution of both reactions (I) and (II) to charge storage is deduced from the shape of the initial discharging patterns of the sample, as Fig. 5 shows. The plateau typical of Fe discharge (see Fig. 2) is here distorted by Ti_2Ni which, unlike Fe, has a sloping discharge profile which extends to −0.700 V (or above) versus HgO [16]. Fig. 5 also indicates a very low interaction between the two redox systems.

During subsequent cycles, the pattern of Fig. 5 tended to flatten, but the capacity settled only slightly above that of samples B and C (see Table 3). As a matter of fact, if the charge presumably stored on Fe, as determined from the limit capacity of either sample B or C is withdrawn from the limit capacities of this electrode, the charge stored on hydrogen may be inferred. Now, the values obtained by this procedure, reported in the last column of Table 3 (the former datum was corrected by the Fe contribution using values given by sample B, the latter was corrected by C) do indicate that this IMC did not contribute much to charge storage. However, during galvanostatic discharging, it was noted that sample D vigorously outgassed for a long time: in other words, hydrogen was loaded during charging but discharged

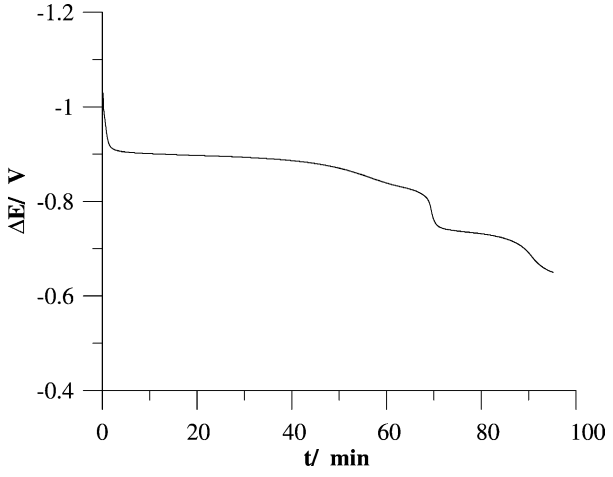

Fig. 5. ΔE vs. time pattern of sample D during discharge ($I = -20$ mA).

Table 3
Maximum charge capacity of electrodes D–L

Electrode	Charging mode (fast/slow)	Extracted charge (mA h g^{-1})	Storage on hydrogen[a] (%)
D (Ti_2Ni + Fe)	Fast	165	≤9
D (Ti_2Ni + Fe)	Slow	224	9/24
E (TiFe + Fe)	Fast	215	18/30
E (TiFe + Fe)	Slow	290	30/41
F (TiFe + Fe)	Slow	273	27/38
G ($Ti_{40}Ni_{60}$ + Fe)	Fast	222	21/32
G ($Ti_{40}Ni_{60}$ + Fe)	Slow	242	16/29
H ($Ti_{40}Ni_{60}$ + Fe)	Fast	180	3/17
H ($Ti_{40}Ni_{60}$ + Fe)	Slow	213	5/20
I ($Ti_{70}Ni_{30}$ + Fe)	Fast	231	24/35
I ($Ti_{70}Ni_{30}$ + Fe)	Slow	275	26/38
L ($Ti_{70}Ni_{30}$ + Fe)	Fast	251	20/40
L ($Ti_{70}Ni_{30}$ + Fe)	Slow	347	41/51

[a] Hypothesized.

inefficiently, since most of it escaped electrochemical oxidation.

3.2.2. Behaviour of samples E and F (TiFe + Fe)

Fig. 6 shows the evolution of charge storage in sample E with the number of charging–discharging cycles. The graph was obtained as above (Figs. 1 and 3); empty and full symbols have the usual meanings; the dotted curve represents the activation pattern of sample C (Ti + Fe, see Fig. 3) for comparison.

Activation was initially sluggish, but later the capacity increased to nearly 50% above that of sample C. This observation is quantified by the maximum storage data listed in Table 3. Examining the data of the last column of Table 3, we see that between 30 and 41% of the charge extracted after slow charging was presumably due to hydrogen, which means that the intrinsic hydrogen capacity achieved here by TiFe may be estimated from 150 to 200 mA h g^{-1}.

The behaviour of sample E was substantially reproduced by another TiFe + Fe specimen (sample F), which was mainly activated by slow charging runs, and later submitted to X-ray analysis (see below).

3.2.3. Behaviour of samples G and H ($Ti_{40}Fe_{60}$ + Fe)

As already noted in Section 2, compound $Ti_{40}Ni_{60}$ is not a true IMC but, according to the manufacturer's specifications, an alloy precursor "made by sintering a blend of powders of the component metals to achieve alloying by diffusion; the resultant cake is ground and sieved to the required particle size". The charge storage behaviour of this precursor, used alone, was examined first. Thus, a sample having dimensions and powder contents similar to those of Table 1 was submitted to a series of charging–discharging cycles according to the usual procedure: the results are summarised in the insert of Fig. 7. The two curves represent the discharging ΔE versus time patterns of the first and ninth cycles, respectively; a storage increase took place from the former to the latter, but the charge actually stored, by reason of the very low discharging current (I = 1.5 mA), was far too low (from <1 to <3 mA h g^{-1}).

Fig. 7 shows the evolution of charge storage with number of cycles for the composite $Ti_{40}Ni_{60}$ + Fe (G). This sample activated very quickly: during the first ≈20 cycles, its capacity nearly doubled that of sample C (dotted line in Fig. 7): the limit capacities achieved within this range are listed in Table 3 in which (last column) the percentage of presumed storage on hydrogen is also reported.

At the 24th cycle, capacity decreased and then dropped sharply. The same behaviour was exhibited by sample H: limit capacities were similar but, starting from the 33rd cycle (again after prolonged charging), capacity dropped.

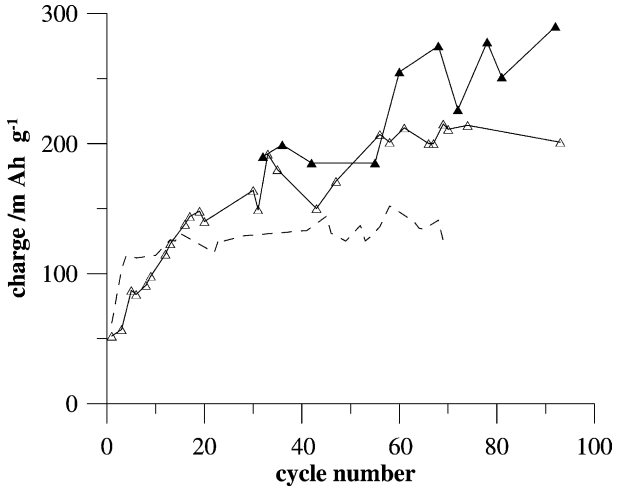

Fig. 6. Evolution of charge capacity with the number of cycles of sample E (TiFe + Fe). Plain curves: full and empty symbols have the usual meaning. The dotted curve represents the analogue pattern of sample C.

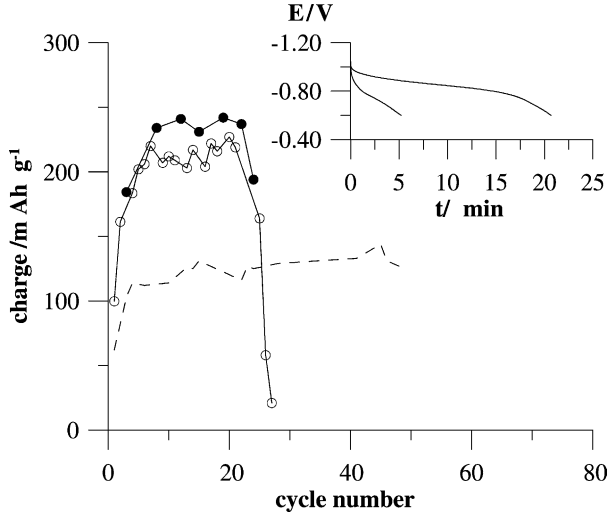

Fig. 7. Evolution of charge capacity with the number of cycles of sample G ($Ti_{40}Ni_{60}$ + Fe). The dotted curve represents the pattern of sample C. The insert represents the discharging pattern (I = 1.5 mA) of a mere $Ti_{40}Ni_{60}$ electrode at the first and the ninth cycle, respectively.

Table 4
Charge capacity of electrodes G–H resulting from two-step extractions

Electrode	Cycle no.	Charging mode (fast/slow)	First extraction		Second extraction		Total charge (mA h g^{-1})
			I (mA)	Charge (mA h g^{-1})	I (mA)	Charge (mA h g^{-1})	
G	25	Slow	25	164	10	94	253
G	27	Fast	40	21	10	225	246
G	29	Slow	10	207	10	49	256
H	33	Fast	40	116	10	127	243
H	37	Slow	20	213	10	59	272
H	39	Slow	40	66	10	209	275
H	43	Slow	10	242	10	30	272

The capacity drop observed in both samples was due to the fact that, for still unexplained reasons, the stored charge could no longer be extracted at relatively high current (e.g. $I = 40$ mA). This observation was substantiated by the capacity data of both electrodes in the later cycles, as shown in Table 4. Not only did the extracted charge depend inversely on discharging current but, on submitting each sample to later discharging at a lower current value ($I = 10$ mA), ≈1 h after the former, a residual charge content reciprocal with that extracted previously was systematically found, so that total storage was approximately constant. In other words, the active material of the electrode maintained a definite ability to store charge, but lost other electrochemical features such as the ability to sustain fast charge extraction.

3.2.4. Behaviour of samples I and L ($Ti_{70}Fe_{30}$ + Fe)

The compound $Ti_{70}Fe_{30}$, used alone, showed no ability to store charge, more or less as previously seen for pure $Ti_{40}Ni_{60}$ (Fig. 7, insert).

Instead, Fig. 8 shows that sample I, although activated more slowly than sample C (dotted curve), reached the capacity previously attained by E (TiFe + Fe electrode) in a few dozen cycles. Table 3 quantifies this observation by indicating the storage on hydrogen predictably ranging between 24 and 38% of full capacity.

This result was confirmed and improved by sample L. Submitted to a series of slow charging runs more numerous than before, sample L not only showed continuously increasing capacity but (after slow charging) attained a storage on hydrogen estimated between 41 and 51%, corresponding to an intrinsic $Ti_{70}Ni_{30}$ capacity of ≈220–300 mA h g^{-1}. Other than showing no loss of the ability to sustain relatively fast discharging rates (up to 300 mA g^{-1}), both samples I and L were charged–discharged efficiently, like as the Fe electrode (Fig. 2) and exhibited flat discharging patterns. As a typical instance, Fig. 9 compares the highest capacity pattern of sample L with the analogue of sample B (Ni + Fe), which had about the same Fe content.

3.3. X-ray analysis

X-ray analysis was performed on samples F, H and L. The activated electrodes were examined in their charged state,

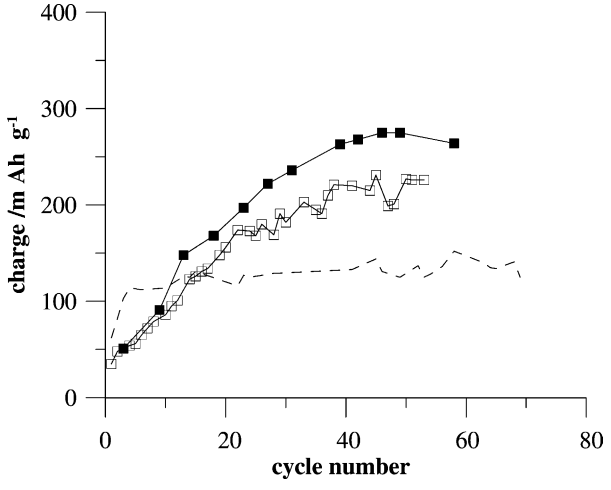

Fig. 8. Evolution of charge capacity with the number of cycles of sample I. Full and empty symbol have the usual meaning: the dotted curves represent the analogues pattern of sample C.

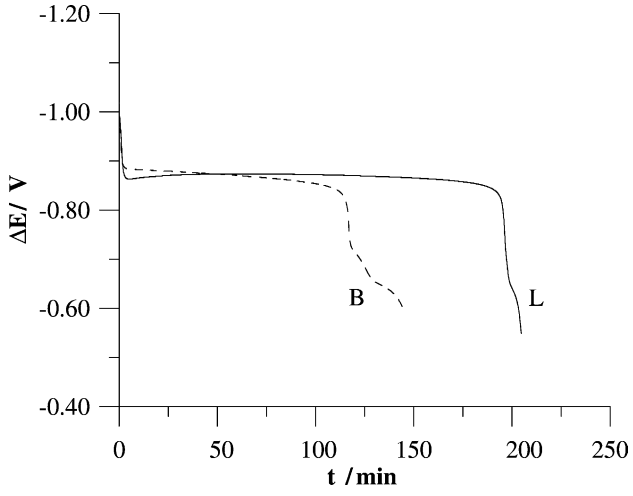

Fig. 9. Comparison of discharging patterns ($I = 20$ mA) of maximum capacity of samples L (plain curve) and B (dotted curve), respectively.

after prolonged electrolytic reduction: the delay occurring between the end of electrolysis and the beginning of X-ray spectrum acquisition was $\leq$0.5 h.

The X-ray pattern of Fig. 10 was obtained from sample F (TiFe + Fe) when it had attained a charge capacity >270 mA h g^{-1}. Whereas the virgin electrode gave only the signals of its components (Ni foam, TiFe and Fe), most of the TiFe now appeared to have been converted into $TiFeH_2$ the peaks of which, at angles 38.50, 38.59, 40.81 and 43.12 (2θ), differed from those of the parent IMC, not only in position and relative intensity, but also in the lack of diffraction at 78.77. Fig. 10 also shows important new peaks at angles 30.11, 30.43, 56.95 and 62.51 (2θ), all due to Fe oxides such as magnetite (Fe_3O_4) which, progressively forming after the repeated charging–discharging runs in the inner layers of the electrode, were no longer suitable for electrochemical reduction.

The spectrum of virgin sample H ($Ti_{40}Ni_{60}$ + Fe) gave only the patterns of its component metals (Ti, Ni, Fe), without any signals from intermetallic phases which, if present, should have been invisible to X-rays, due to their low crystallinity. The main changes revealed in this spectrum by the electrolytic process were considerable drops in peak intensity for both Ti and Fe (whereas the Ni pattern intensity remained almost unchanged) and the appearance of strong magnetite signals. When the activated H electrode was submitted to SEM analysis, the surface structure indicated not only stochastic distribution of the metal powder components, but also several patches of microcrystalline aggregates, as shown in Fig. 11A. Now, the elemental EDAX analysis of these aggregates systematically gave the almost exclusive presence of Ti and Fe, in the atomic ratios typical of TiFe intermetallic phases, as shown in Fig. 11B.

Fig. 12A shows the X-ray spectrum of virgin sample L ($Ti_{70}Ni_{30}$ + Fe) which again indicated only the presence of Ni, Fe and Ti. The $Ti_{70}Ni_{30}$ powder compound alone, although marketed as an alloy, did reveal the same patterns (except for peak intensity ratios) of the $Ti_{40}Ni_{60}$ alloy precursor, with no evidence of intermetallic phases.

Fig. 12B shows the profound changes induced by the electrolytic cycles: other than a significant relative decrease in Ti and Fe peaks with respect to Ni peak and the appearance of the magnetite pattern, a number of new peaks occurred, the identification of which is not allowed by the existing literature.

Furthermore, the significant peaks at low angles are metastable, since they fade and modify with time, as Fig. 12C shows (this spectrum was recorded $\approx$22 h after spectrum 12A). This behaviour may be due to the decomposition of some unidentified hydride phase.

4. Discussion

When used alone for hydrogen storage, the alloys selected for this study presented partial or total inhibition which, for all of them except Ti_2Ni, was in some way overcome in the mixed IMC + Fe electrodes.

It therefore seems convenient to start the discussion with Ti_2Ni, in order to explain why sample D, unlike the others, gave very low storage on hydrogen, owing to the large H_2 loss paralleling electrochemical discharging. The phenomenon of hydrogen escape by a non-electrochemical recombination step is not uncommon (it occurs, for instance, at Pd hydride discharged by low current density [18]). In the present case, the phenomenon may be ascribed to a non-positive interaction between Fe and Ti_2Ni, perhaps due to the excessive particle size of the latter (fine grinding of Ti_2Ni is problematic [16]). Therefore, during discharge, most of the current is supplied by Fe oxidation, whereas the inserted hydrogen which diffuses from the bulk to the IMC surface recombines at Ni islands and even more at adjacent Fe particles, which act as recombination sites, since atomic hydrogen is more unstable on Fe than on Ni.

As regards the alloys giving storage increments when mixed with Fe, TiFe will be examined first. The problems related to the electrolytic hydriding of this compound have recently been studied, and show that:

- TiFe is totally inhibited to hydrogen absorption in strong alkaline electrolytes, but may be partially hydrided by cycling in aqueous carbonates [19];
- the cycle life of the activated compound is greatly increased by additions of 15–25% Fe [20].

Loading with 40% active Fe gave an immediate activation route, which avoided the cumbersome cycling in aqueous carbonates.

During charging, Fe mixes with the IMC and also acts as a her catalyst, which induces surface TiFe reduction and hydrogen insertion; during discharging, Fe oxidation is a buffer which delays the onset of TiFe repassivation indefinitely.

It is quite probable that these effects by Fe again played a basic role in the activation of $Ti_{40}Ni_{60}$ and $Ti_{30}Ni_{70}$, although other phenomena also take place in these compounds.

Thus, for samples G and H, the apparent charge capacity drop after a given number of cycles (Fig. 7) and the subsequent inverse dependence of the charge on the extraction current (Table 4), already suggest the occurrence of significant changes in the active material. This had already been substantiated by the SEM and EDAX analyses, which revealed surface patches of likely TiFe composition. They probably affected the original electrode response of Fe (a fast surface reaction) and, in the meantime, stored and/or released charge as hydrogen (a bulk, diffusion-limited reaction). The formation of intermetallic bonds is not uncommon in electrochemistry (electrolytic alloy deposition has long been known), but the electrolytic formation of Ti–Fe bonds is rather

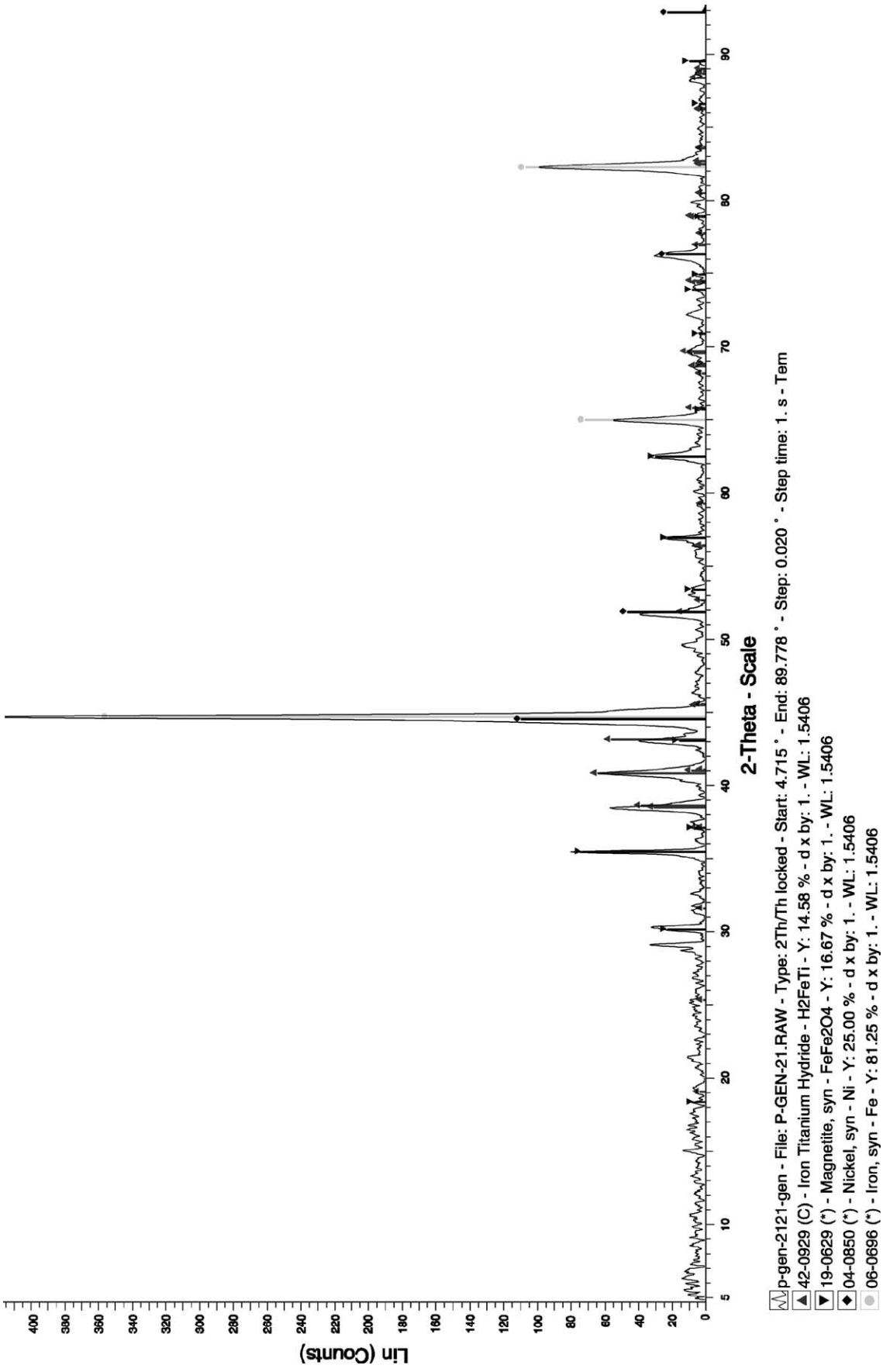

Fig. 10. X-ray diffraction pattern of the activated F sample.

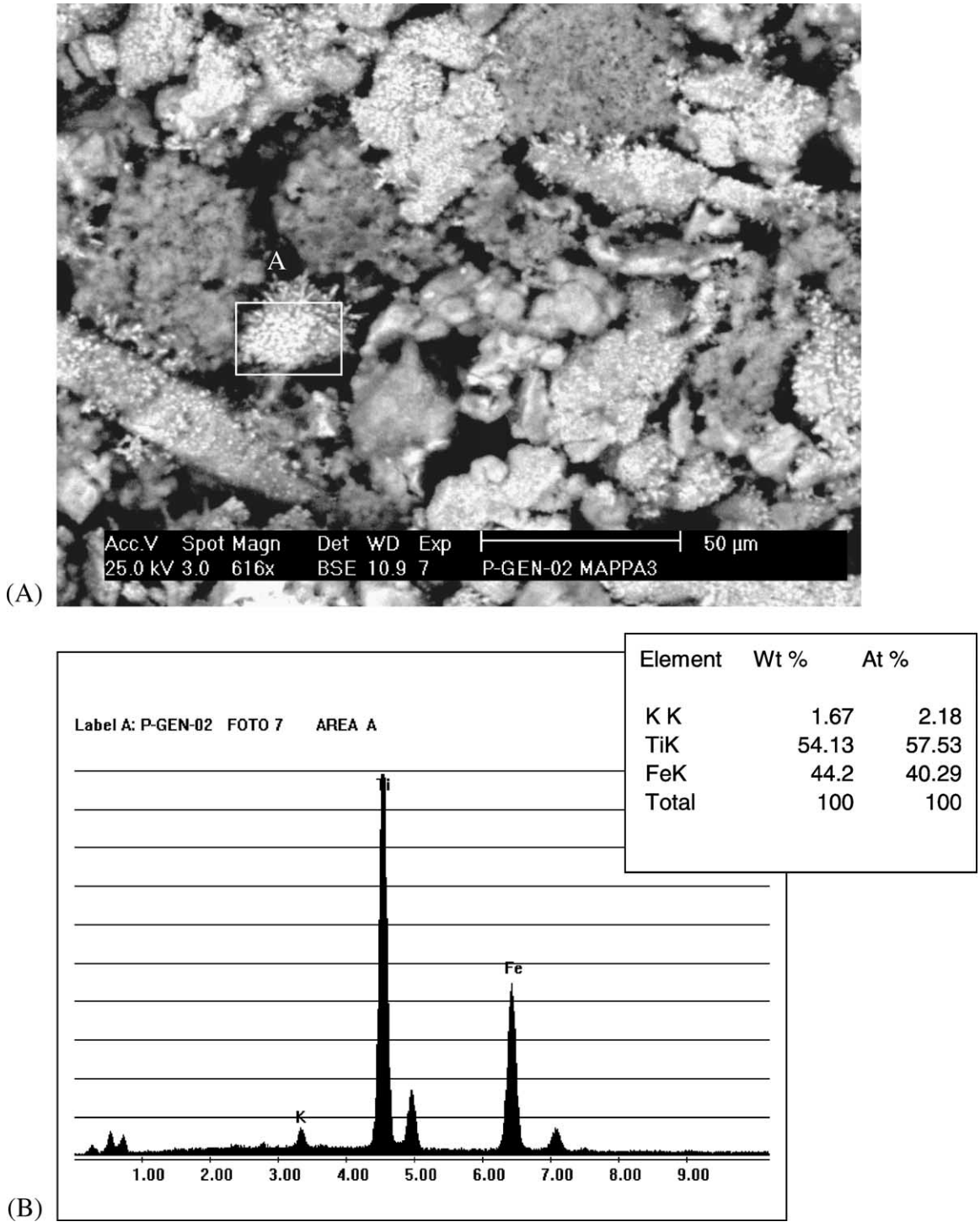

Fig. 11. (A) SEM image of the activated sample H: the square indicates the microcrystalline aggregate analysed by EDAX. (B) EDAX analysis of the microcrystalline aggregate.

surprising, owing to the strong passivation of Ti and the practical impossibility of Ti electrodeposition from aqueous electrolytes.

However:

- it has recently been shown [21] that the passivity of Ti in alkaline media may be overcome after prolonged cathodic reduction, with conversion of surface oxides into Ti hydride;
- in a strongly alkaline electrolyte, the characteristics of an aprotic medium are approached.

Therefore, during repeated discharging runs, some Fe, Ti, or both (perhaps as mixed hydroxides) may be dissolved near

the powder electrode particles, and are then plated during reduction, with the formation of intermetallic patches.

As regards samples I and L ($Ti_{70}Ni_{30}$ + Fe), it must be noted that the charge capacity of, for instance, sample L (Table 3) cannot be explained by storage on Fe, even in the unlikely case of attaining the theoretical capacity of Fe, since X-ray analyses showed that 20–30% of Fe present on the ''charged'' sample (Fig. 12B) was in the oxidized magnetite form. The obvious consequence is that a fraction of the charge capacity of I and L must due to hydrogen, presumably inserted in some intermetallic phase alloyed during the activation process.

Two compositions, $Ti_{40}Ni_{60}$ and $Ti_{70}Ni_{30}$, giving similar X-ray diffraction patterns (not unlike those of a mixture of the component metals), in the same experimental conditions did behave quite differently. On one hand, this highlights the fact that the state and reactivity of an alloy precursor are quite different from those of a simple mechanical mixture of metals. On the other hand, it is stressed here that the surface properties of the material represent the key to the reaction pathway and/or possible alloying within a mixed powder electrode.

In conclusion, when loading Fe in composite electrodes to activate IMCs reluctant to hydrogen absorption, our data indicate that the achievement of either positive or negative results depends on the nature of the chosen IMC.

Thus, Ti_2Ni + Fe and TiFe + Fe represent two limit situations of electrochemical incompatibility and good compatibility between IMC and Fe.

Good electrochemical compatibility as regards charge storage were observed for $Ti_{40}Ni_{60}$ + Fe and $Ti_{70}Ni_{30}$+ Fe,

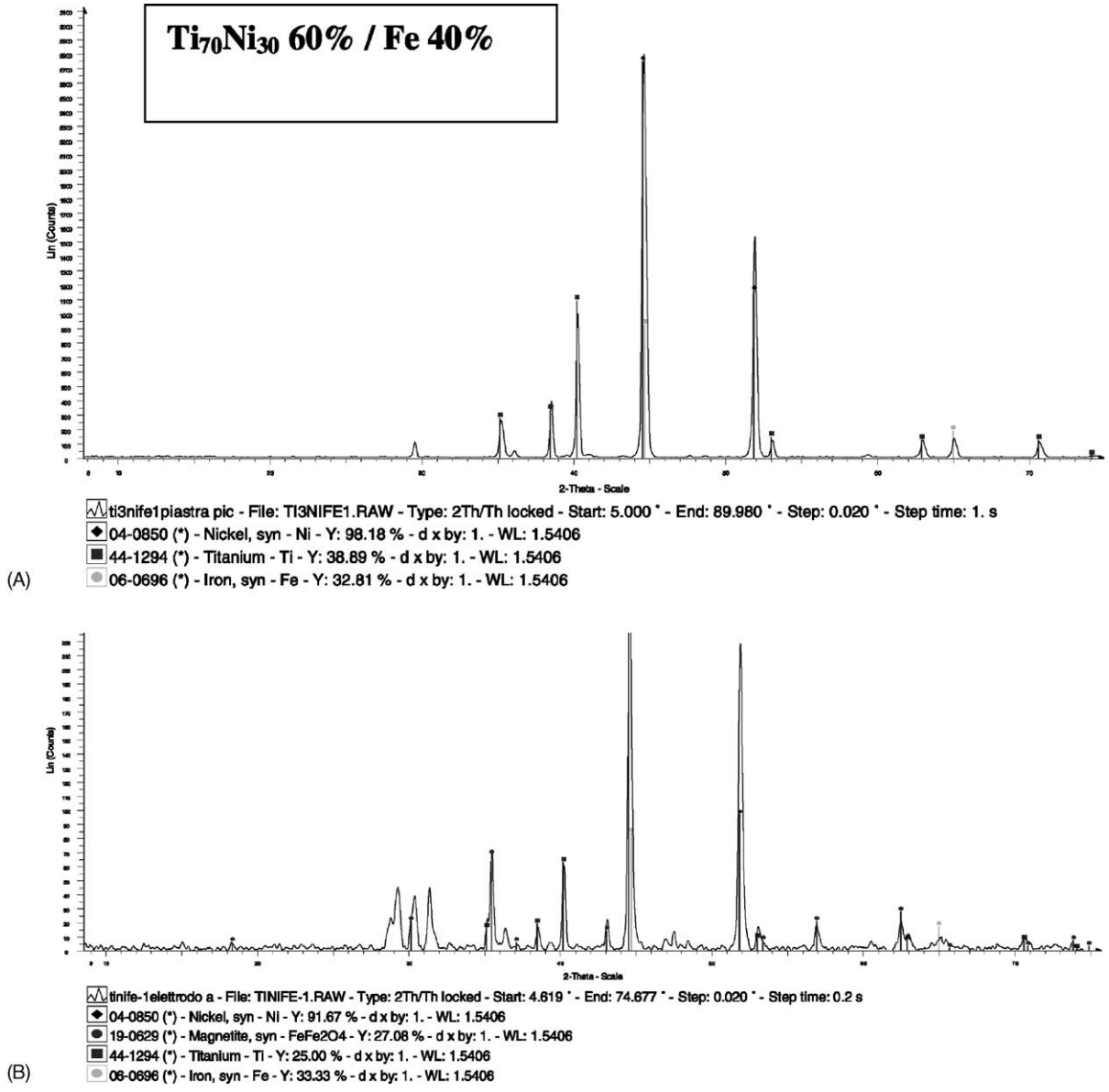

Fig. 12. X-ray diffraction pattern of sample L. (A) Virgin sample; (B) activated sample in the charged state; (C) activated electrode after ≈1 day from the end of the electrolysis.

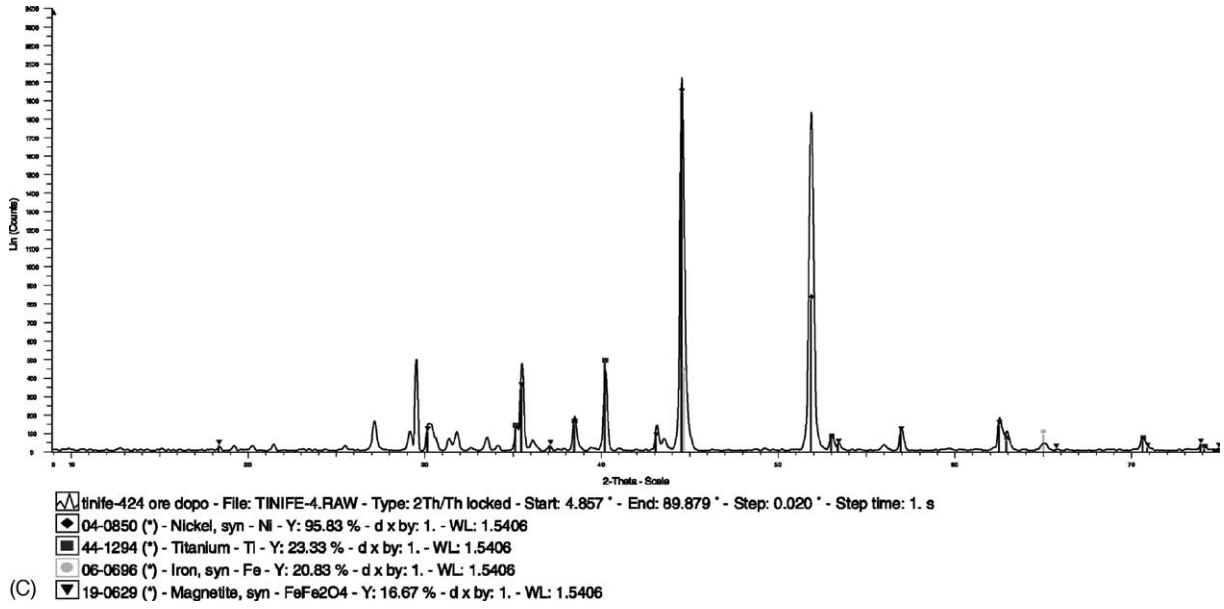

Fig. 12. (*Continued*).

but chemical reactivity within the respective component was also tested: the effect of this unpredicted phenomenon played a positive role only for the latter composition.

References

[1] J.J. Willems, K.H.J. Buschow, J. Less-Common Met. 129 (1987) 13.
[2] J. Kleperis, G. Wojcik, A. Czerwinski, J. Skowronski, M. Kopczyk, M. Beltowsla-Brzezinka, J. Solid State Electrochem. 5 (2001) 229.
[3] G. Sandrok, S. Suda, L. Schlaphach, Hydrogen in intermetallic compounds. II. Applications, in: L. Schlaphach (Ed.), Topic in Applied Physics, vol. 67, Springer, Berlin, 1992, pp. 240–244.
[4] G. Sandrok, in: P.D. Bennet, T. Sakai (Eds.), Proceedings of the Symposium on Hydrogen and Metals Hydride Batteries, Battery Division, The Electrochemical Society, vols. 94–127, Pennington, 1994, p. 1.
[5] D. Berudt, Maintenance-Free Batteries, Research Studies Press Ltd., Taunton, 1997, p. 398.
[6] C. Jordy, M. Latroche, A. Percheron-Guegan, J.C. Achard, J. Bouet, B. Knosp, B. Pichon, Z. Phys. Chem. 185 (1994) 119.
[7] B. Luan, N. Cui, H.K. Lin, H.J. Zhao, S.X. Dou, J. Power Sources 55 (1995) 197.
[8] M. Matsuoka, T. Kohno, C. Iwakura, Electrochim. Acta 38 (1993) 787.
[9] L. Sum, H. Lin, D.H. Brandhurst, S. Don, Electrochem. Solids-State Lett. 2 (4) (1999) 164.
[10] K. Petrov, A.A. Rostarni, A. Visintin, S. Srinivasan, J. Electrochem. Soc. 141 (1994) 1747.
[11] C.H. Hamman, A. Hamnett, W. Vielstich, Electrochemistry, Wiley, New York, 1998, p. 360.
[12] S. Hills, J. Electrochem. Soc. 112 (1965) 1048.
[13] S.V. Falk, A.J. Salkind, Alkaline Storage Batteries, Wiley, New York, 1969, pp. 613–619.
[14] P.R. Vassie, A.C.C. Tseung, Electrochim. Acta 21 (1976) 299.
[15] I. McBreen, Secondary batteries—introduction, in: J.O.M. Bockris, B.E. Conway, E. Yeager, R.E. White (Eds.), Comprehensive Treatise of Electrochemistry, vol. 3, Plenum Press, New York, 1981, pp. 325–326.
[16] E.W. Justi, H.H. Ewe, A.W. Kalberlah, N.M. Saridakis, M.H. Schaefer, Energy Conversion 10 (1970) 183.
[17] B. Luan, N. Cui, H. Zhao, H.K. Lin, S.X. Don, J. Power Sources 55 (1995) 101.
[18] A. Czerwinski, G. Maruszczak, M. Zelazowska, Pol. J. Chem. 67 (1993) 2037.
[19] M. Bernardini, N. Comisso, G. Davolio, G. Mengoli, J. Electroanal. Chem. 487 (2000) 1.
[20] N. Comisso, G. Davolio, E. Soragni, G. Mengoli, J. Electroanal. Chem. 512 (2001) 92.
[21] R.J. Elias, H.L. Corso, J.L. Gervasoni, Int. J. Hydrogen Energy 27 (2002) 91.